



RESEARCH ARTICLE

Time-resolved fluorescence anisotropy with Atto 488-labeled phytochrome Agp1 from *Agrobacterium fabrum*

Afaf Elkurdi¹ | Gernot Guigas² | Latifa Hourani-Alsharafat¹ | Patrick Scheerer³  | Gerd Ulrich Nienhaus^{2,4,5,6}  | Norbert Krauß¹  | Tilman Lamparter¹ 

¹Botanical Institute, Karlsruhe Institute of Technology (KIT), Karlsruhe, Germany

²Institute of Applied Physics, Karlsruhe Institute of Technology (KIT), Karlsruhe, Germany

³Charité – Universitätsmedizin Berlin, corporate member of Freie Universität Berlin and Humboldt-Universität zu Berlin, Institute of Medical Physics and Biophysics, Group Structural Biology of Cellular Signaling, Berlin, Germany

⁴Institute of Biological and Chemical Systems, Karlsruhe Institute of Technology, Eggenstein-Leopoldshafen, Germany

⁵Institute of Nanotechnology, Karlsruhe Institute of Technology, Eggenstein-Leopoldshafen, Germany

⁶Department of Physics, University of Illinois at Urbana-Champaign, Urbana, Illinois, USA

Correspondence

Tilman Lamparter, Botanical Institute, Karlsruhe Institute of Technology (KIT), Fritz-Haber-Weg 4, D-76131 Karlsruhe.

Email: tilman.lamparter@kit.edu

Abstract

Phytochromes are photoreceptor proteins with a bilin chromophore that undergo photoconversion between two spectrally different forms, Pr and Pfr. Three domains, termed PAS, GAF, and PHY domains, constitute the N-terminal photosensory chromophore module (PCM); the C-terminus is often a histidine kinase module. In the *Agrobacterium fabrum* phytochrome Agp1, the autophosphorylation activity of the histidine kinase is high in the Pr and low in the Pfr form. Crystal structure analyses of PCMs suggest flexibility around position 308 in the Pr but not in the Pfr form. Here, we performed time-resolved fluorescence anisotropy measurements with different Agp1 mutants, each with a single cysteine residue at various positions. The fluorophore label Atto-488 was attached to each mutant, and time-resolved fluorescence anisotropy was measured in the Pr and Pfr forms. Fluorescence anisotropy curves were fitted with biexponential functions. Differences in the amplitude A_2 of the second component between the PCM and the full-length variant indicate a mechanical coupling between position 362 and the histidine kinase. Pr-to-Pfr photoconversion induced no significant changes in the time constant t_2 at any position. An intermediate t_2 value at position 295, which is located in a compact environment, suggests flexibility around the nearby position 308 in Pr and in Pfr.

KEYWORDS

biliprotein, flexibility, Pr Pfr

INTRODUCTION

Light is sensed by organisms via photoreceptors, specific signaling proteins carrying a light-absorbing organic chromophore as a cofactor.¹ When the conjugated π -electron system of the chromophore absorbs light, the photoreceptor

protein switches from an active to an inactive state or vice versa. This switching is usually coupled to protein conformational changes in the photoreceptor. Phytochromes incorporate a linear tetrapyrrole as the chromophore, which can be either biliverdin, phycocyanobilin, or phytychromobilin. In phytochromes, protein conformational changes

Afaf Elkurdi and Gernot Guigas contributed equally.

This is an open access article under the terms of the [Creative Commons Attribution](https://creativecommons.org/licenses/by/4.0/) License, which permits use, distribution and reproduction in any medium, provided the original work is properly cited.

© 2023 The Authors. *Photochemistry and Photobiology* published by Wiley Periodicals LLC on behalf of American Society for Photobiology.

associated with their signaling function are triggered by isomerization around a double bond between rings C and D of the chromophore. Photoconversion is coupled to characteristic spectral changes between the long-lived or stable red light-absorbing form Pr and the far-red light-absorbing form Pfr. In phytochrome Agp1 of *Agrobacterium fabrum* and most other phytochromes, Pr is the dark-stable form.²⁻⁴ The photoproduct Pfr undergoes slow dark conversion back to Pr. The second phytochrome of *Agrobacterium fabrum*, Agp2, is a so-called bathy phytochrome, in which dark conversion proceeds from Pfr-to-Pr, and the dark-stable form is the (bathochromic, red-shifted) Pfr form.⁵

Light-induced protein conformational changes are associated with differential interaction with other proteins and modulation of enzyme activity. Plant phytochromes interact in a Pfr-specific manner with nuclear translocation proteins⁶ and PIF transcription factors,⁷ which are important for Pfr-specific nuclear transfer and gene transcription. Modulation of enzyme activity is found in bacterial and fungal phytochromes, most of which carry a C-terminal histidine kinase module. Such modules are found in many prokaryotic and some eukaryotic signaling systems. The universal key step is an autophosphorylation on a conserved histidine residue, which is followed by a trans-phosphorylation to a so-called response regulator.⁸ However, the role of histidine kinases in phytochrome signaling is still unclear. In Agp1, autophosphorylation is strong in the Pr and weak in the Pfr form.⁹ This pattern is found in other bacterial phytochromes¹⁰; the reverse pattern, that is low activity in Pr and high activity in Pfr, has also been observed.¹¹ Agp1 has a rather low-temperature maximum of its kinase activity (25°C), suggesting that Agp1 may act as a thermosensor.¹⁰

Typical bacterial phytochromes are composed of five protein domains. The N-terminal photosensory core module (PCM) consists of an N-terminal PAS domain, a central GAF domain, and a PHY domain. The C-terminus of the PHY domain is linked to the histidine kinase module, which consists of a dimerization/histidine phosphotransfer (DHp) domain and an ATPase domain (see Figure 1A,B). The ring A vinyl side chain of the biliverdin chromophore is covalently bound to a cysteine residue N-terminal of the PAS domain, the major part of the chromophore interacts with amino acids of the GAF domain. PAS and GAF domains of all phytochromes interact via a knotted structure.¹² A part of the PHY domain, the so-called tongue, binds to the chromophore pocket on the GAF domain. This establishes a signaling pathway from the chromophore via the tongue to the PHY domain and finally to the histidine kinase. During photoconversion, the tongue undergoes pronounced secondary structure changes. It forms a β -hairpin structure in the Pr form,¹² which converts into a single α -helical element and loop structures

in the Pfr form.¹³ Based on multiple crystal structures of Agp1-PCM in the Pr form, we assume that a hinge in the GAF-PHY-connecting helix and the tongue of the PHY domain confer flexibility between the PHY domain and the rest of the PCM (the PAS-GAF bidomain). This hypothesis is based on the observation that the bending angles formed within the PAS-GAF-connecting helix in the different crystals cover a strikingly wide range.¹² This flexibility is apparently lost in the Pfr form, as all Pfr structures contain a straight GAF-PHY-connecting helix with no evidence of flexibility yet. The proposed flexibility of the PHY domain in PCM structures is illustrated in Figure 1C by a comparison of two Agp1 PCM crystal structures and the proposed loss of flexibility is exemplified in Figure 1D by a comparison of two bathy phytochrome PCM structures in the Pfr form. The relevant angle in the long GAF-PHY connecting helix differs significantly between the two Pr structures and is more or less the same in the two selected bathy phytochrome structures, which are representative here of all Pfr structures.¹² The transition from β -sheet to α -helix in the tongue is most likely the cause for the switch in flexibility of the PHY domain in PCM structures.¹⁴ Most phytochrome crystal structures are from the N-terminal PCM, which lacks the histidine kinase.¹³

In the full-length protein, the presence of the histidine kinase module leads to additional structural and functional complexity. Differences between Pr and Pfr that are found in PCM variants are not necessarily the same in the full-length protein. In each subunit, the DHp substrate domains of histidine kinases act via strong dimer interaction sites. For Agp1, dimerization via histidine kinase has been shown by cross-linking experiments¹⁵ and PELDOR distance measurements.¹⁶ It is clear that dimerization by the histidine kinase will restrict the movement of the PHY domain around the hinge, although subtle movements may be possible. According to the PCM crystal structures, two GAF domains or two PHY domains can also form specific dimer contacts. However, dimer contacts within the PCM are weaker than those in the histidine kinase because the PCM appears as a mixture of monomers and dimers in biochemical characterizations. In PCM crystals, the subunits are sometimes arranged in a parallel and sometimes in an antiparallel manner, which is only possible if the contacts are weak. For the PCM variants of the phytochromes Agp1 and Cph1, dimer formation is much stronger in the Pfr than in the Pr form.¹⁷ According to recent EM structural models, the dimer arrangement of plant phytochromes is more complex as the domains of each subunit in the dimer do not interact with the partner domain of the other subunit.¹⁸ However, full-length bacterial phytochrome structures point to a stretched parallel arrangement,¹⁹ suggesting that histidine kinase subunits have parallel arrangements in all non-plant phytochromes.

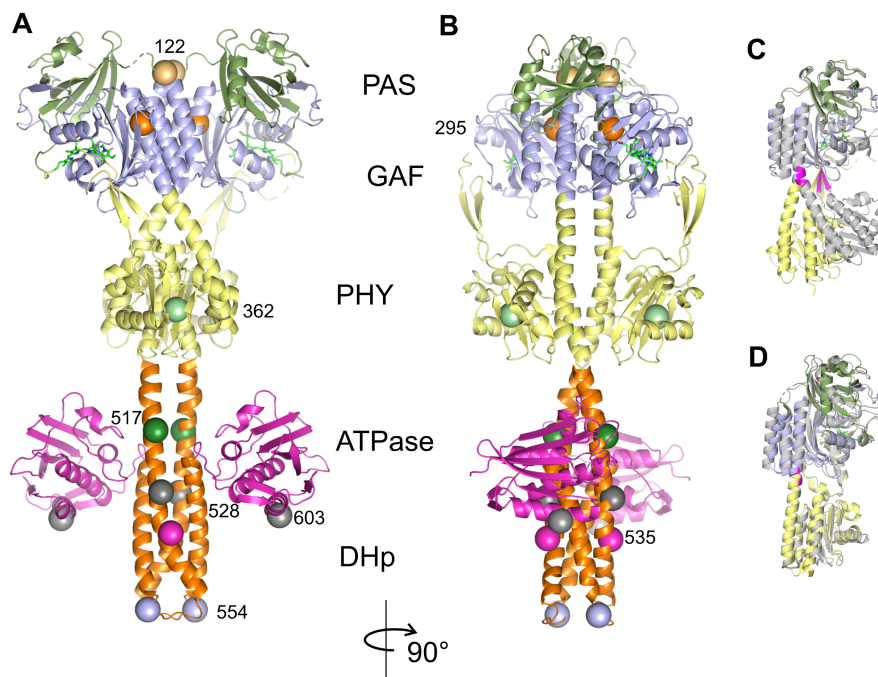


FIGURE 1 (A, B) Model of the full-length Agg1 dimer. The PCM structure was taken from PDB code 6R27, the histidine kinase dimer structure was constructed with SwissModel using the structure from *Thermotoga maritima*, PDB code 2C2A, as a template. The mutant positions to which Atto labels were introduced are indicated by spheres in different colors, the numbers stand for the positions within the protein. PAS, GAF, and PHY domains are colored in green, blue, and yellow, respectively; DHp and ATPase domains of the histidine kinase are stained in orange and magenta, respectively. (C) Superimposed monomer Pr structures of two different Agg1 PCM crystals from PDB code 5HSQ (gray) and PDB code 6R27 (various colors). The hinge is labeled in magenta. Both models are aligned according to their PAS/GAF bidomains, the orientation of the PHY domains and the angle in the GAF-PHY-connecting helix are largely different. They are representative of the large variations in these bending angles observed for Pr structures. (D) Superimposed Pcm Pfr crystal structures of Agg2 (PDB Code 6G1Y, various colors) and *Pseudomonas aeruginosa* BphP (PDB code 3NHQ), with the same view and alignment as for the Agg1-PCM structures in panel C. All Pfr structures have a straight GAF-PHY helix.

Information on the flexibility of protein regions can be gained from time-resolved fluorescence anisotropy measurements of fluorophore-labeled constructs.^{20,21} In such measurements, the fluorescence label is excited by a short, linearly polarized pulse of laser light to select a sub-ensemble whose transition dipoles are preferentially aligned along the direction of the excitation light. This photoselection disappears due to rotational dynamics, which can be assessed by measuring the intensity of fluorescence light polarized parallel and perpendicular to the incident beam as a function of time. From these two intensities, we calculate the anisotropy, which reports on the rotational dynamics but not on the fluorescence decay. For our system, the time dependence of the anisotropy is well fitted with a biexponential function, representing fast rotation of the fluorophore tethered to the proteins and slower rotation due to protein motions in the vicinity of the fluorophore. Our aim here was to use fluorescence anisotropy measurements to assess whether protein flexibility changes during Pr-to-Pfr photoconversion in full-length Agg1 and, furthermore, how the Pr-specific hinge is involved in signal transduction from the PCM to the histidine kinase. To address

these questions, we labeled Agg1 with the maleimide-functionalized Atto 488 dye, which allows it to be coupled to cysteine side chains. We took advantage of eight Agg1 mutants that had been generated for MTSL (1-oxyl-2,2,5,5-tetramethylpyrroline-3-methyl-methanethiosulfonate) spin labeling for pulsed EPR-DEER structural studies,¹⁶ with each mutant having a single cysteine for labeling at a specific position on the protein (Figure 1A,B).

MATERIALS AND METHODS

Agg1 mutants

All proteins used in this study had a C-terminal 6-His tag for affinity purification and were expressed in *E. coli* X11-blue. The generation of mutants is described in.¹⁶ The C295 mutant is equivalent to C279A, but retains the chromophore binding Cys 20 and a Cys at position 295 used for dye labeling. All other mutants are based on the full-length protein Agg1 C279A C295S (Cys 279 mutated to Ala and Cys 295 to Ser), which has only the

chromophore binding Cys-20 as a single Cys. This double mutant was used to generate S122C, A362C, K517C, H528C, R535C, K554C, and R603C, in which the amino acids at the indicated positions were replaced by Cys. The mutant Agp1-A362C-PCM was generated from the full-length version Agp1-A362C by truncating the polypeptide chain to amino acids 1–503 so that it contains only the PAS, GAF, and PHY domains. Notably, it is identical in length to the Agp1 variants that were used for crystallization and other biochemical experiments.^{12,22}

Protein expression and purification

For the fluorescence-based assay, Agp1 variants were first expressed in *E. coli* XL1-Blue and then purified as apoproteins, following previous work.⁹ Bacterial strains with the desired expression vector were grown in 3 L LB medium with 0.3 mM Amp at 37°C until the cell density reached an OD_{600nm} of 0.6–0.8. Protein expression was induced by 300 μM IPTG (isopropyl-1-thiol-β-D-galactopyranoside) and incubated at 18°C until the OD_{600nm} reached ~2. The cells were harvested by centrifugation at 9000g for 10 min (4°C), and the pellet was washed in 200 mL basic buffer (300 mM NaCl, 50 mM Tris/Cl, 5 mM EDTA, pH 7.8) and centrifuged again at 9000g for 10 min. The resulting pellet was suspended in 20 mL basic buffer. Cells were extracted using a French Pressure Cell at a pressure of 20,000 psi. The lysed cells were centrifuged at 12,000g for 30 min in order to recuperate the soluble protein in the supernatant. Protein was precipitated using 50% or 66% saturated ammonium sulfate for full-length or PCM proteins, respectively.

The pellet was then dissolved in washing buffer (basic buffer with 10 mM imidazole and without EDTA), and the sample was centrifuged again. The resulting supernatant was applied to a nickel affinity chromatography column (Qiagen), which binds the His-tagged Agp1 proteins. The Nickel column was first equilibrated with 200 mL washing buffer (basic buffer with 10 mM imidazole). The loaded column was then washed with 1 L washing buffer, then with high NaCl buffer (1 M NaCl in washing buffer), and finally with 2 L washing buffer until all the free and unspecifically bound proteins were washed out of the column. The apoprotein was eluted with the elution buffer (wash buffer, imidazole increased to 250 mM). The elution steps were followed by measuring the absorption at 280 nm. Protein-containing samples were pooled and precipitated by mixing with 3.3 M ammonium sulfate in 50 mM Tris/Cl, 5 mM EDTA, pH 7.8, followed by centrifugation at 12,000g for 20 min. The resulting pellet was dissolved by adding 1–2 mL basis buffer and centrifuged again. Finally, the supernatant was divided into 100 μL aliquots, frozen in liquid nitrogen, and stored at –80°C for

further use. Both Agp1 and Agp2 proteins were essentially pure after purification, as confirmed by SDS-PAGE results. Their concentrations varied between 0.1 and 0.4 mM. The purified proteins were then used for the assembly and the labeling process as below.

Biliverdin assembly and Atto-488 labeling, phosphorylation

For de-acidification of biliverdin, 100 μL of a 20 mM biliverdin (Sigma-Aldrich) solution, dissolved in DMSO, was loaded onto a 1 mL SepPak C18 cartridge (Waters) that had been equilibrated in water. The column was washed with 20 mL water, and the bound biliverdin was eluted with 2–4 mL methanol. Biliverdin was concentrated to dryness in a spin vacuum and finally dissolved in DMSO to a concentration of 10 mM.²³

Agp1 apoprotein had a starting absorbance, A_{280nm} ≈ 1, equivalent to ca. 10 μM. Prior to the addition of biliverdin at room temperature, 10 mM of TCEP (tris(2-carboxyethyl) phosphine) was added to the protein. Biliverdin was added at a final concentration of 30 μM, and the solution was incubated for 20 min. This ensures that all apoproteins have a bound biliverdin, as spectroscopic changes due to binding are generally complete within 2 min. To remove excess biliverdin and TCEP, 0.5 ml of the samples were passed through NAP-5 columns (GE Healthcare) that have been equilibrated with basic buffer. Proteins were eluted basic buffer according to manufacturer's instructions.

The maleimide derivative of Atto 488 (Atto-Tec), which attaches to thiol groups of cysteine residues, was used for fluorophore labeling. Atto 488 stock solutions (10 mM) were prepared in DMSO and stored at –80°C until further use. Labeling and spectroscopic measurements were performed in green safe light or in the dark to maintain the Pr (dark ground) state. Assembly and Atto 488-labeling of Agp1 mutants (see Results section) were performed similarly. Immediately thereafter, Atto 488 was added to the purified holoprotein in a twofold molar excess, as any delay results in a reduced level of labeling. The samples were incubated either for 2 h at RT, or overnight at 4°C in darkness under constant shaking, if not used directly for further measurements. Subsequently, free Atto 488 was removed by running the mixture through a NAP-5 size exclusion column and, afterward, by repeated dilution and concentration by ultrafiltration (membrane filter units Amicon® Ultra -15, Ultracel – 30K; Merck Millipore Ltd.) to remove traces of free biliverdin or Atto 488. The samples were then characterized by UV/Vis spectroscopy.

Pr-to-Pfr and Pfr-to-Pr photoconversions were performed with 655 nm red and 780 nm far-red light-emitting

diodes, respectively, next to the measuring microscope. Light intensities were $100\mu\text{molm}^{-2}\text{s}^{-1}$ for red light and $200\mu\text{molm}^{-2}\text{s}^{-1}$ for far red. Autophosphorylation experiments were performed essentially as described previously.¹⁰

Fluorescence anisotropy

Time-resolved fluorescence anisotropy was measured using a confocal microscope (Microtime 200, Picoquant) equipped with a time-correlated single photon counting (TCSPC) data acquisition system. The samples were excited with linearly polarized light of 488-nm wavelength from a picosecond pulsed laser (LDH-P-C-485; Picoquant) operating at 16 MHz with an average power in the microwatt range. The polarization extinction ratio (PER) of the laser was $>10:1$. The laser light was focused on the samples with a water immersion objective (UPLSAPO 60XW, $60\times/1.2\text{ W}$; Olympus). The fluorescence emission was collected by the same objective, focused onto a pinhole of $50\mu\text{m}$, passed through a 520/35 nm bandpass filter (AHF), and separated into two beams with orthogonal polarization by a polarizing beam splitter cube. The photon counts of the parallel and perpendicular polarized emissions of a sample were detected by two single-photon avalanche photodiodes (SPCM-AQR-14; PerkinElmer Optoelectronics). The arrival time of each photon relative to the exciting laser pulse was recorded using a HydraHarp 400 TCSPC module (Picoquant). Fluorescence decay curves were constructed using the SymPhoTime software (Picoquant).

The time-resolved fluorescence anisotropy was calculated as

$$r(t) = (I_{\parallel} - G \cdot I_{\perp}) / (I_{\parallel} + 2 \cdot G \cdot I_{\perp}) \quad (1)$$

Here, $I_{\parallel}(t)$ and $I_{\perp}(t)$ denote the fluorescence intensities emitted by the sample with parallel and perpendicular polarization, respectively, with respect to the excitation light. The grating factor G is an instrument correction factor accounting for the polarization bias of the detection and was determined with calibration measurements with aqueous solutions of the dye Atto 488. The value of G was around 1.06. The instrument response was included in the data fitting using an iterative deconvolution analysis.²⁴ In this analysis, fluorescence anisotropy decay curves were modeled with a sum of two exponential functions and a constant,

$$r(t) = A_1 \cdot e^{-t/t_1} + A_2 \cdot e^{-t/t_2} + r_{\infty} \quad (2)$$

The relaxation times t_1 and t_2 reflect the fast rotation of the fluorophore around its attachment point (t_1) and the dynamics of the protein segment to which the fluorophore

is attached (t_2). A_1 and A_2 are the corresponding amplitudes. The rotation of an entire phytochrome is expected to occur on a time scale of 100 ns, which could not be reliably explored here due to the short lifetime (4 ns) of Atto 488. The anisotropy therefore appears to decay to a constant end value r_{∞} . We did not observe any correlations between the parameters.

For all phytochrome variants and mutants, the initial anisotropies $r(t = 0\text{ s})$ exhibited relatively low values around 0.14–0.17. By contrast, pure Atto 488 dye showed an initial anisotropy of 0.33 in a highly viscous glycerol–water mixture (glycerol 90% mass) where fast rotation of the dye was not possible. From this, we conclude that the low initial anisotropies of phytochromes occurred due to very fast rotational dynamics of the Atto 488 that could not be resolved in the measurement.

RESULTS

Mutants and autophosphorylation

For fluorescence anisotropy measurements, we used Agp1 mutants S122C, C295, A362C, K517C, H528C, R535C, K554C, and R603C of the full-length protein¹⁶ in which a cysteine residue is located at the positions indicated for fluorescence labeling with Atto 488. The cysteine at position 20, which is present in wild type and all mutants, is the site of covalent chromophore attachment of Agp1.^{9,25} The labeling positions are shown in the full-length structural model of Agp1 (Figure 1A,B). In the wild-type Agp1 protein, the autophosphorylation activity of the histidine kinase is downregulated upon Pr-to-Pfr photoconversion. In order to test the functionality of the mutants, we compared autophosphorylation of Pr and Pfr of the Atto-labeled mutants with the (unlabeled) wild-type. In these experiments, Pfr autophosphorylation activity of the wild-type was approximately half that of Pr (Figure 2). In earlier studies, the Pr: Pfr phosphorylation ratio was higher, around 4:1.⁹ The lower ratio in the present studies could be due to slightly different purification or assembly. The same Pr: Pfr pattern and a similar magnitude of autophosphorylation were found for S122C, C295, and A362C. In K517C and R535C the Pr autophosphorylation was only 60% and 30%, respectively, of the type, respectively, but significant differences between both forms with high Pr and low Pfr were obtained. In the R554C mutant, phosphorylation was reduced as compared to the wild type and differences between Pr and Pfr were only small. For R603C, the pattern was comparable with the wild type, but overall levels were slightly reduced. Thus, mutations within the histidine kinase module reduced

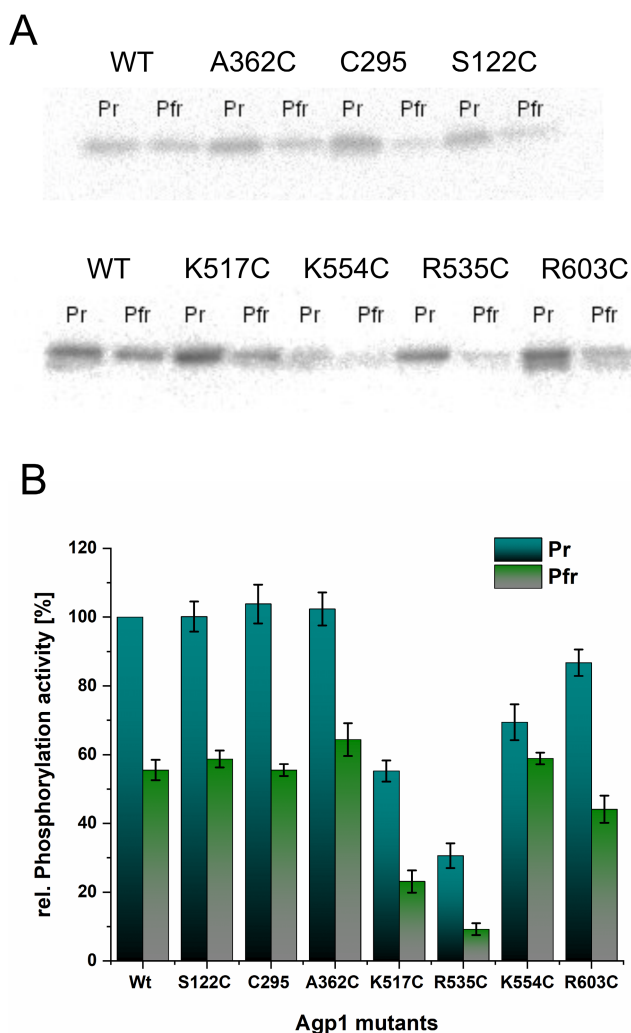


FIGURE 2 Phosphorylation pattern of Agp1 wild-type and Atto-labeled mutants. (A) After autophosphorylation in Pr or Pfr, samples were subjected to SDS-PAGE and proteins were blotted onto a membrane. Mutant names are given by the labels. All mutants were labeled with Atto 488, wild type was not labeled. The blots were recorded with a phosphoimager. (B) Quantification of staining intensities as in (A), mean values \pm SE of three independent phosphorylation experiments. Each blot always included a wild-type sample; the value of wild-type Pr was set to 100%.

the autophosphorylation activity, whereas mutations in the PCM had no effect. However, it should be noted that specific mutants in the PCM region of cyanobacterial phytochrome Cph1 had a major effect on autophosphorylation.¹⁷ No autophosphorylation was detected in the H528C mutant (data not shown), since His 528 is the substrate for autophosphorylation. Based on phosphorylation patterns, we assume that all Atto 488 labeled mutants except R535C undergo almost the same light-induced conformational changes as the wild-type protein and can therefore represent the wild-type protein in the anisotropy measurements presented below.

Fluorescence anisotropy measurements

In time-resolved fluorescence anisotropy measurements, the sample is exposed to picosecond pulses of polarized laser light. Fluorophores that have their transition dipole moments aligned to the electric field vector of the light have a higher probability of being excited, leading to photoselection of a sub-ensemble of fluorophores with a preferential direction. Rotation of the fluorophores during the time that they are in the electronically excited state continuously reduces the photoselection. For quantitative analysis, it is customary to calculate the anisotropy, $r(t)$ (Equation 1), which cancels out intensity changes due to the fluorescence decay, showing only those due to rotational dynamics. Accordingly, the magnitude of the anisotropy is maximal at early times, and its decay can be observed on the nanosecond time scale, that is, as long as excited fluorophores exist. The decay kinetics, which provide information about the motion of the (tethered) fluorophore and the molecule to which it is attached, are typically described by exponential functions.

For fluorescence anisotropy, the Atto 488-labeled Agp1 mutant samples were first measured in the Pr dark state. They were converted then to Pfr by saturating them with red light and measured again. To ensure that the laser flashes did not significantly change the Pr/Pfr levels, UV/vis spectra were taken before and after the anisotropy measurements. For each mutant, we repeated the measurements three or four times with protein samples that were purified and labeled independently. As an example, we show the fluorescence and anisotropy decay curves of the Atto 488-labeled mutant K517C in Figure 3A,D, respectively. The anisotropy decays for all mutants in the Pr and Pfr states are shown in Figure 4.

The anisotropy was calculated up to 21.4 ns, above which the fluorescence emission was too low for satisfactory signal-to-noise ratio. All anisotropy data could be well fitted with Equation 2. The associated residuals are shown in Figure 3B,C. They were between -3 and 3 and were similar for other mutants. Mono-exponential fits were inappropriate and yielded systematic deviations, as judged from the large residuals; fits with three decay components did not give better results than biexponential fits. The values of t_1 were between 0.4 and 1.1 ns, while the values of t_2 were in the range of 4–8 ns. Simulating and fitting decay curves of different lengths and appropriate noise levels, we could see that the limited analysis window (21.4 ns) only minimally affected the fit results for t_2 (below 1% of the value).

First anisotropy decay component

The bar charts in Figure 5A–D show the parameters obtained from fitting the anisotropy decays with Equation 2,

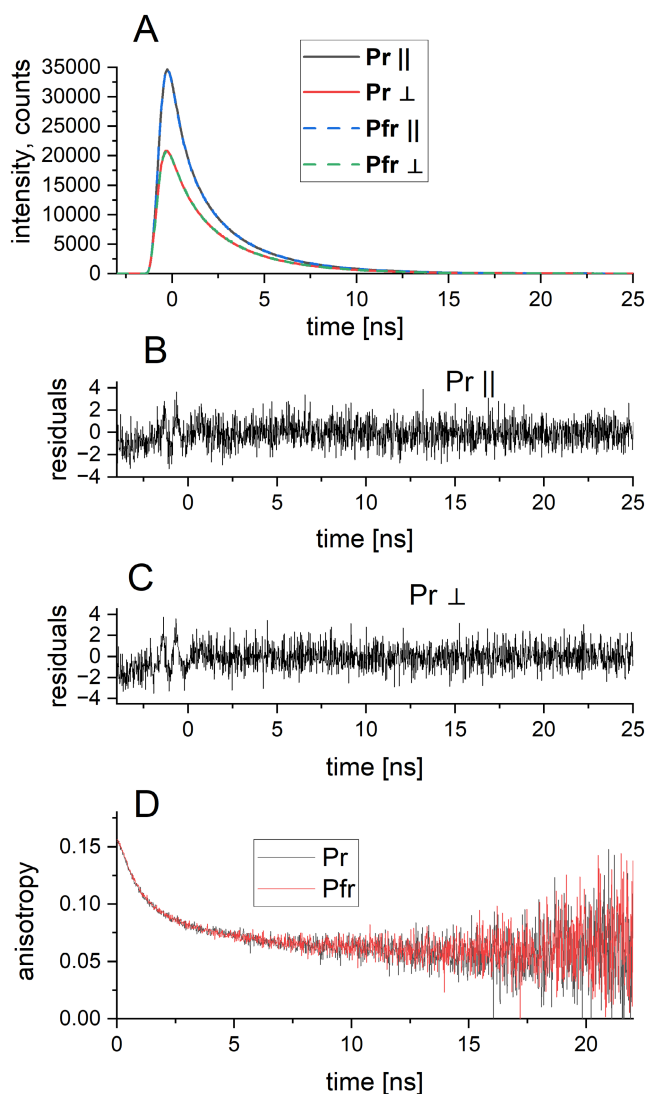


FIGURE 3 Time-resolved fluorescence intensity and anisotropy of Atto 488-labeled Agp1 K517C in the Pr and Pfr states. (A) Time-resolved fluorescence emission, measured parallel (\parallel) or perpendicular (\perp) to the orientation of the excitation E-vector. (B) and (C), residuals between data and fit for Pr and Pfr. (D) Anisotropy of Pr (black) and Pfr (red), calculated from the intensities in panel (A) with Equation 1 and biexponential fits to the Pr (black) and Pfr (red)

that is, the amplitudes A_1 and A_2 of the two exponential components and of the respective time constants t_1 and t_2 , averaged over all measurements. Green or red colors in the squares in Figure 5E–H indicate whether the mean values of two mutants differ by more or less than three standard deviations (SDs) by a green or red field, respectively. $A > 3$ SD difference (green) was considered as significant. The comparisons between Pr and Pfr of each sample are given in the diagonal in a darker color.

The amplitudes of the first component, A_1 , which reflect the extent of fluorophore rotational mobility, were between

0.015 and 0.06 (Figure 5A,E). The Pr and Pfr measurements of each sample were very similar to each other; no significant differences were observed. The R603C mutant had the lowest value around 0.015. Since standard deviation (SD) and standard error (SE) of this sample were high, the difference in the other samples was not significant. The highest A_1 values were obtained for Pr and Pfr of the C295 mutant. The SD and SE values of the C295 Pfr measurements were small and a significant difference was obtained between C295 on one side and A362C, H528C, R535C, K554C, R603C, or A362C-PCM on the other side. Position 295 is at the N-terminus of the long GAF-PHY-connecting helix.

The time constants of the first component, t_1 , were in the range of 0.4–1.1 ns (Figure 5C), which is characteristic of rotational diffusion of the fluorophore around its attachment site.^{26,27} Atto 488 freely diffusing in aqueous solution had a time constant t_1 of 0.44 ± 0.02 ns (resulting from a fit with a mono-exponential model). Thus, the rotational mobility of the fluorophore bound to Agp1 is somewhat slowed in some mutants, due to the covalent attachment and interactions with surrounding amino acids.

Although the mean values were variable, the differences between samples were usually not significant (Figure 5G). Significant Pr/Pfr differences were also not observed. The Pr of H528C and R603C was the only pair that differed in these measurements.

The overall impression from the first decay component is that C295 and H528C have t_1 and/or A_1 values above those of the other mutants. Both positions are on a long helix, C295 at the N-terminus of the PAS/GAF helix and H528 on the helix connecting the PHY domain and the histidine kinase.

Second anisotropy decay component

The averages of the time constant t_2 and the corresponding amplitude A_2 were characterized by small experimental errors and were significantly different for most samples (Figure 5F,H). However, no significant differences between Pr and Pfr were found.

The highest amplitudes A_2 with around 0.11 were found for R663C and A362C-PCM. Quite remarkably was the second lowest A_2 with 0.057 obtained for A362C (Figure 5F). For the other parameters, the differences between proteins with and without histidine kinase were insignificant (Figure 5E,G,H). The lowest A_2 with 0.054 was obtained for K517C.

The time constants t_2 were in the range of 4–8 ns (Figure 5D). This range is characteristic for the mobility of local regions of the protein.²⁷ Rotations of the entire Agp1 dimer in solution would be much slower. According to Stokes's law for rotation, the time constant scales

with the volume and thus approximately with the mass.²⁶ Therefore, the time constant of rotation of the Agp1 dimer (170 kDa) would be ca. 100 ns, as estimated by rescaling

data from bovine serum albumin, which has 66 kDa and a time constant of rotational diffusion of 41.7 ns.²⁶ The monomeric PCM variant with 55 kDa has an estimated time

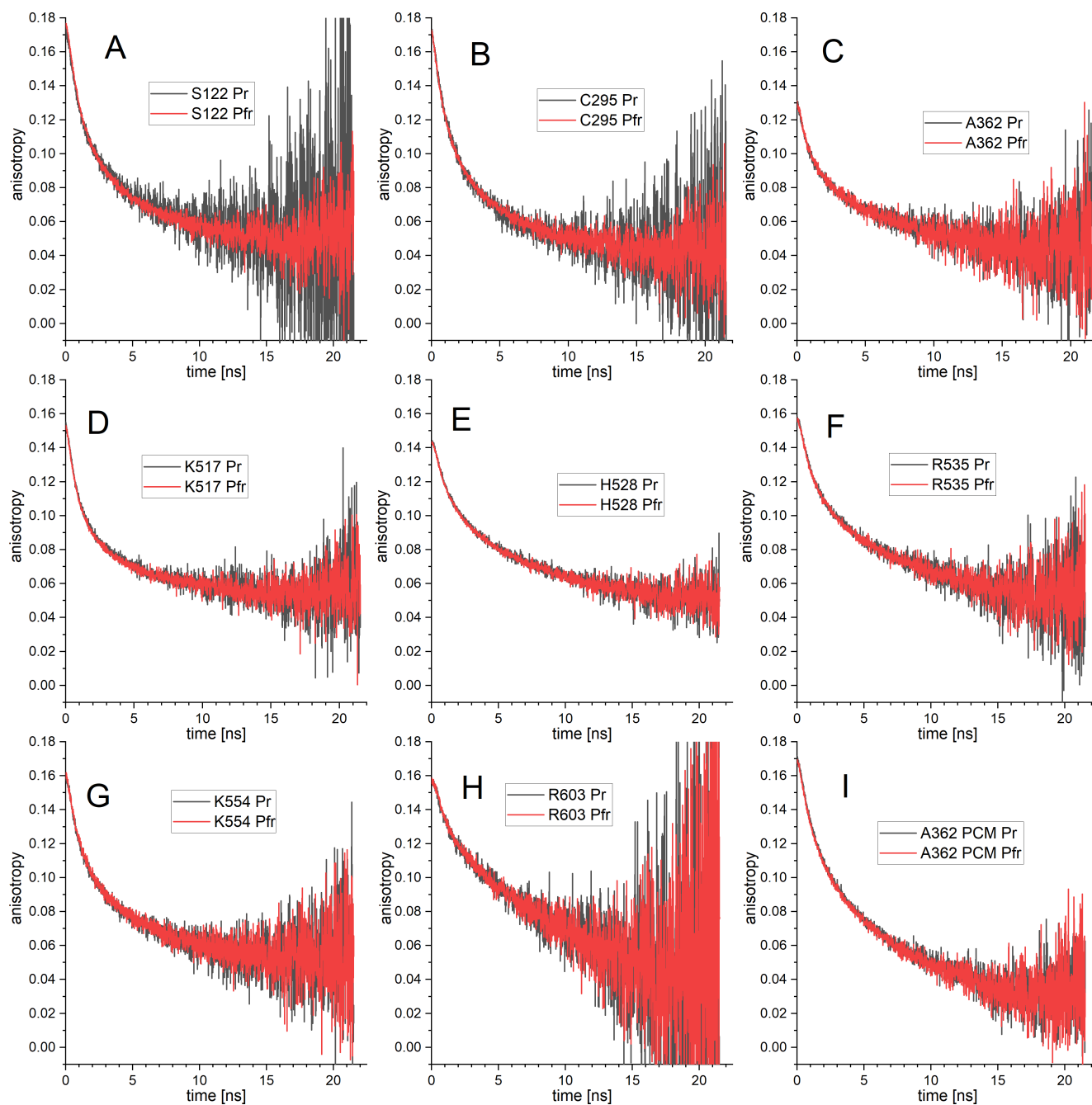
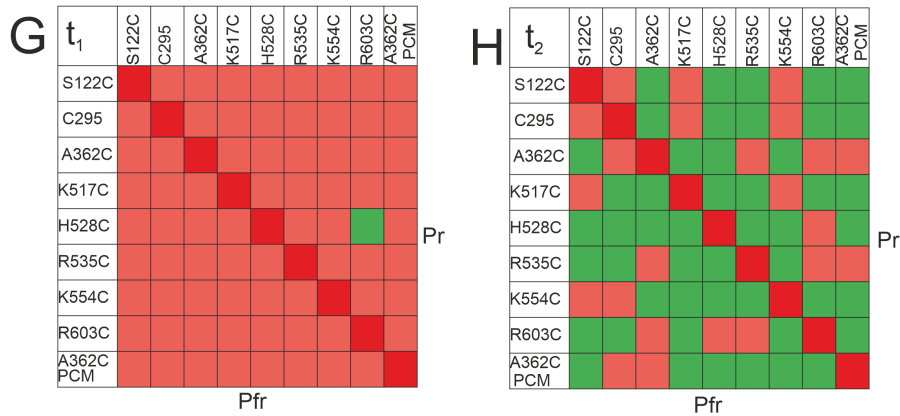
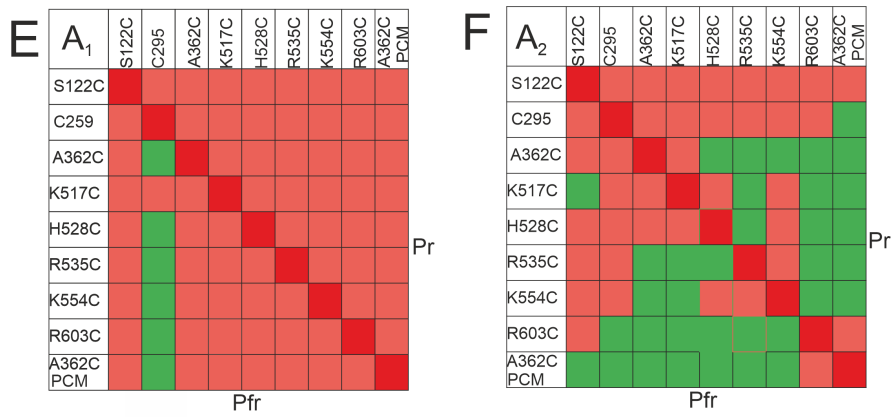
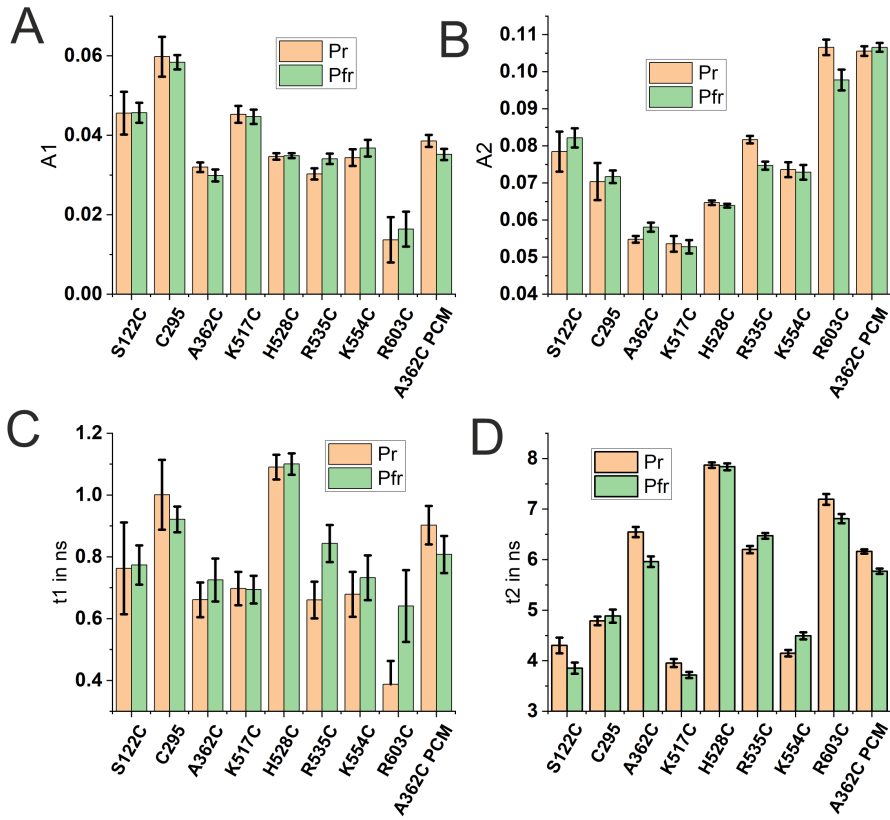


FIGURE 4 Fluorescence anisotropy decay of Agp1 mutants, averaged over three or four measurements each in the Pr and Pfr states. The labeling positions are given in each legend. All variants are based on the full-length protein except A362C-PCM, which is presented in panel I.

FIGURE 5 Amplitudes and time constants of fluorescence anisotropy of Atto-488 labeled Agp1, as obtained by fitting the data in Figure 4 with biexponential functions (Equation 2). The protein mutants were labeled with Atto 488 at a cysteine, as indicated by the mutant nomenclature. Mean values \pm SE. (A) A_1 and (B) A_2 in the Pr and Pfr forms. (C) t_1 and (D) t_2 in the Pr and the Pfr forms. (E, F, G, H) Show for A_1 , A_2 , t_1 , and t_2 whether differences between mutant pairs are significant (green) or not significant (red). Comparison of Pr states are on the upper right triangle, Pfr on the lower left. The diagonals show Pr–Pfr differences. The criterion for significance is that the mean values differ by more than three SD.



constant of ca. 40 ns, still far above the measured t_2 values. In fact, measurement of the rotational dynamics of these proteins is not possible with Atto 488, as its fluorescence decay time of 4.11 ns limits anisotropy measurement to <22 ns (see above).

The highest values for t_2 at 7.9 ns were again found for H528C, significantly different from all other mutants except R603C, which had the second highest values. H528 is the phosphorylation position of Agp1. The position with the lowest t_2 values was K517, which like H528 is located on the long PHY-DHp connecting helix $\alpha 15$ just three turns away from H528. The t_2 values of K517C were significantly lower than those of S122C, A362C, H528C, and K554C.

Difference between Agp1-A362C PCM and full-length protein

The A362C mutant was measured as the full-length protein and as PCM, the N-terminal chromophore module without histidine kinase. Comparison of data from both constructs unravels the effect of the histidine kinase on fluorophore mobility at position 362. For t_1 , t_2 , and A_1 , there were no significant differences between PCM and full-length protein (Figure 5A,C,E,G). However, for A_2 , there were large differences between full-length A362C and A362C-PCM (Figure 5B,F). These differences show clearly that the rotational dynamics of the local region around position 362 are influenced by the histidine kinase.

DISCUSSION

This study was carried out to determine whether regions of phytochrome undergo changes in mobility upon Pr-to-Pfr photoconversion. The mode of signal transmission from the N-terminal PCM to the C-terminal histidine kinase of a bacterial phytochrome is not yet understood. There are five different crystal structures of Agp1-PCM proteins and the coordinates of eight monomers have been determined independently (Ref. 12 and manuscript submitted). Comparison of these structures indicated that there is a hinge between the long GAF-PHY-connecting helix $\alpha 9$ (289–334) and the tongue of the PHY domain. Movement around this hinge appears to be lost upon conversion to Pfr, as shown in Figure 1C,D. Accordingly, we expect that the PCM variant shows flexibility between the PHY and the GAF-PAS domains in the Pr form and a loss of flexibility in the Pfr form. In the long helix $\alpha 9$, the hinge is located within a small region centered at position 308 (see also Figure 1A–D).

Fluorescence anisotropy experiments were performed with Agp1 mutants that allowed coupling of a

maleimide-derivatized fluorophore at eight specific positions along the protein. For each construct, a detailed comparison was made between Pr and Pfr. In addition, a comparison between the PCM Agp1 variant and the full-length version of mutant A362C was performed. The labeling positions closest to the proposed hinge are position 295, located at the N-terminus of the long GAF-PHY helix ($\alpha 9$), and position 362, which lies on a β -sheet within the PHY domain. Between position 362 and helix $\alpha 9$ there are three helices $\alpha 10$ (338–344), $\alpha 11$ (346–356), and $\alpha 15$ (481–547), which form polar and hydrophobic side chain contacts to the β -sheet and the long helix $\alpha 9$. One of the three helices, $\alpha 15$, is the C-terminal helix of the PHY domain which extends to the histidine kinase in the full-length protein. Therefore, the amino acid at position 362 could be vibrationally coupled to both the DHp of the histidine kinase and to helix $\alpha 9$.

Although A_2 and t_2 values were significantly different between the different mutants, the Pr and Pfr data were not significantly different for any mutant and any parameter. Since the errors are small and the mean values of Pr and Pfr are very similar, we conclude that the flexibility of the protein region does not change during photoconversion at either selected position or that there are only minor changes that are probably not relevant. A flexibility change around a hinge close to position 308 would have been detected by the mutant C295 and/or by the mutant A362C.

Most protein samples that were measured here are full-length Agp1 carrying the C-terminal histidine kinase. In the full-length protein, a movement around position 308 could be restricted by the strong dimer formation of the kinase region. The A362C mutant was however measured also as PCM without histidine kinase. In this fragment, flexibility would not be restricted by the histidine kinase, but there are no Pr: Pfr differences in this fragment either. We note that the A_2 values were drastically different between the A362C PCM and the corresponding full-length protein. This difference tells us that anisotropy measurements at position 362 are sensitive against the presence or absence of histidine kinase. On this background, it is even more striking that no significant Pr: Pfr difference was found neither for the PCM nor for the full-length protein.

The t_2 values, which represent the flexibility of the local regions, appear to be highly dependent on the protein surrounding the label position. The lowest t_2 value, indicative of the fastest movement, was obtained for K517C, where the mutated residue is located on the long PHY-DHp helix $\alpha 15$, which is free of side-chain interactions at that position (Figure 1A). Position 517 is part of a short α -helical segment ranging approximately from position 505 to position 518, which does not interact with any other polypeptide strand than the equivalent segment from the other

identical subunit in the parallel dimer. H528C, on the contrary, has the highest t_2 value (close to 8). Position 528 is also on a helix, namely $\alpha 15$. The high t_2 value of H528C is explained by various interactions that the helical segment in $\alpha 15$ C-terminal of position 518 undergoes with various neighboring polypeptide strands from the DHP and ATPase domains and the second dimer subunit. For autophosphorylation, H528 must interact transiently with the ATPase because H528 is the substrate of the kinase. The next label position on helix $\alpha 15$ is 535, for which t_2 is lower than for position 528, indicating that rotational motion is less restricted here than for the substrate site. Different from position 517, however, position 535 belongs to a segment of helix $\alpha 15$ which is involved in interactions with multiple polypeptide segments from the same subunit as mentioned above. High t_2 values at positions 362 can also be explained by interactions between secondary structure elements.

As noted above, this amino acid is part of the central one of three layers of β -strand and α -helices. Positions 122 and 554 are on either end of the dimer structure (Figure 1A), position 122 is on a loop just outside $\alpha 4$ (123–138), and position 554 is on a loop between $\alpha 15$ and $\alpha 16$. In general, loops are more flexible than β -sheets or α -helices, and this explains the low t_2 values of S122C and K554C. C295 is also embedded in a complex structure consisting of three parallel helices, $\alpha 4$, $\alpha 5$ (143–158), and the long helix $\alpha 9$ on which the amino acid is located. Compared with positions 362, 528, 535, or 603, the t_2 value of C295 is rather small. This low t_2 could mean that there is flexibility around the hinge at position 306. The expectation was that the flexibility is present in the Pr form but the hinge is arrested upon photoconversion to Pfr.¹² In the present interpretation, the anisotropy data would indicate that both forms are flexible around position 306. There are several possible explanations for this discrepancy between expectation and data. One possibility could be that the protein structure in solution differs from that in the crystal.

Another interesting observation is the t_2 value at position 603. This is located on the ATPase part of the protein, helix $\alpha 17$. It is connected with $\alpha 18$ and a β -sheet. The high t_2 value suggests that the region is unexpectedly rigid. This is in contrast with proteolysis experiments in which the entire histidine kinase degraded rapidly, whereas the PCM region resisted much longer against the protease.^{15,17}

Fluorescence anisotropy performed at different positions of the protein showed a broad variation in the t_2 and A_2 values. We found correlations between the surroundings of the labeled positions and the t_2 values that can help to understand intramolecular signal transduction. We interpret the t_2 values at C295 as indicating flexibility around the hinge at position 306 in both Pr and Pfr.

CONCLUSIONS

By labeling various Agp1 mutants each via a single cysteine at a defined position with an Atto fluorescent dye, and by measuring time-resolved fluorescence anisotropy of that fluorophore, it was possible to monitor the flexibility of selected protein regions. The originally proposed flexibility change around position 308 of the polypeptide chain during the Pr-to-Pfr conversion was rejected, because no significant changes in A_2 and t_2 values were observed upon photoconversion. It became evident that the histidine kinase is coupled with the region of the PHY domain around position 362, because for the full-length protein and the PCM fragment without histidine kinase significantly different A_2 values were observed. In this way, fluorescence anisotropy contributed to a better understanding of intramolecular signal transmission in a phytochrome.

ACKNOWLEDGMENTS

The work was supported by Deutsche Forschungsgemeinschaft grant LA 799/18-1 to T. L. and KR 2034/1-1 to N. K., through project-ID 221545957 – CRC 1078 “Protonation Dynamics in Protein Function,” subproject B06 (to P.S.), and through the Deutsche Forschungsgemeinschaft (DFG, German Research Foundation) under Germany’s Excellence Strategy—EXC 2008—390540038—UniSysCat. (Research Unit E to P.S.). We also thank the Einstein Center of Catalysis (EC²) funded by the Einstein Foundation Berlin for support (to P.S.). G.U.N. acknowledges funding from the Helmholtz Association, the program Materials Systems Engineering (MSE), and the Karlsruhe School of Optics and Photonics (KSOP). Open Access funding enabled and organized by Projekt DEAL.

CONFLICT OF INTEREST STATEMENT

On behalf of all authors, the corresponding author states that there is no conflict of interest.

ORCID

Patrick Scheerer  <https://orcid.org/0000-0001-5028-2075>

Gerd Ulrich Nienhaus  <https://orcid.org/0000-0002-5027-3192>

Norbert Krauß  <https://orcid.org/0000-0002-7128-4632>

Tilman Lamparter  <https://orcid.org/0000-0003-4327-9737>

[org/0000-0003-4327-9737](https://orcid.org/0000-0003-4327-9737)

REFERENCES

1. Briggs WR, Spudich JL. Weinheim. *Handbook of Photosensory Receptors*. Wiley Press; 2005.
2. Lamparter T, Michael N, Caspani O, Miyata T, Shirai K, Inomata K. Biliverdin binds covalently to Agrobacterium phytochrome Agp1 via its ring a vinyl side chain. *J Biol Chem*. 2003;278(36):33786–33792.

3. Lamparter T, Xue P, Elkurdi A, et al. Phytochromes in *Agrobacterium fabrum*. *Front Plant Sci.* 2021;12:12.
4. Lamparter T, Krauß N, Scheerer P. Phytochromes from *Agrobacterium fabrum*. *Photochem Photobiol.* 2017;93(3):642-655.
5. Karniol B, Vierstra RD. The pair of bacteriophytochromes from *Agrobacterium tumefaciens* are histidine kinases with opposing photobiological properties. *Proc Natl Acad Sci USA.* 2003;100:2807-2812.
6. Hiltbrunner A, Viczián A, Bury E, et al. Nuclear accumulation of the phytochrome A photoreceptor requires FHY1. *Curr Biol.* 2005;15(23):2125-2130.
7. Ni M, Tepperman JM, Quail PH. PIF3, a phytochrome-interacting factor necessary for normal photoinduced signal transduction, is a novel basic helix-loop-helix protein. *Cell.* 1998;95(5):657-667.
8. Robinson VL, Buckler DR, Stock AM. A tale of two components: a novel kinase and a regulatory switch. *Nat Struct Biol.* 2000;7(8):626-633.
9. Lamparter T, Michael N, Mittmann F, Esteban B. Phytochrome from *Agrobacterium tumefaciens* has unusual spectral properties and reveals an N-terminal chromophore attachment site. *Proc Natl Acad Sci USA.* 2002;99:11628-11633.
10. Njimona I, Yang R, Lamparter T. Temperature effects on bacterial phytochrome. *PLoS One.* 2014;9(10):e109794.
11. Bhoo SH, Davis SJ, Walker J, Karniol B, Vierstra RD. Bacteriophytochromes are photochromic histidine kinases using a biliverdin chromophore. *Nature.* 2001;414:776-779.
12. Nagano S, Scheerer P, Zubow K, et al. The crystal structures of the N-terminal photosensory core module of *Agrobacterium* phytochrome Agp1 as parallel and anti-parallel dimers. *J Biol Chem.* 2016;291(39):20674-20691.
13. Schmidt A, Sauthof L, Szczepek M, et al. Structural snapshot of a bacterial phytochrome in its functional intermediate state. *Nat Commun.* 2018;9(1):4912.
14. Takala H, Björling A, Berntsson O, et al. Signal amplification and transduction in phytochrome photosensors. *Nature.* 2014;509(7499):245-248.
15. Noack S, Michael N, Rosen R, Lamparter T. Protein conformational changes of *Agrobacterium* phytochrome Agp1 during chromophore assembly and photoconversion. *Biochemistry.* 2007;46(13):4164-4176.
16. Kacprzak S, Njimona I, Renz A, et al. Intersubunit distances in full-length, dimeric, bacterial phytochrome Agp1, as measured by pulsed electron-electron double resonance (PELDOR) between different spin label positions, remain unchanged upon photoconversion. *J Biol Chem.* 2017;292(18):7598-7606.
17. Esteban B, Carrascal M, Abian J, Lamparter T. Light-induced conformational changes of cyanobacterial phytochrome Cph1 probed by limited proteolysis and autophosphorylation. *Biochemistry.* 2005;44(2):450-461.
18. Li H, Burgie ES, Gannam ZTK, Li H, Vierstra RD. Plant phytochrome B is an asymmetric dimer with unique signalling potential. *Nature.* 2022;604(7904), 127-133. doi:[10.1038/s41586-022-04529-z](https://doi.org/10.1038/s41586-022-04529-z)
19. Wahlgren WY, Claesson E, Tuure I, et al. Structural mechanism of signal transduction in a phytochrome histidine kinase. *Nat Commun.* 2022;13(1), 7673. doi:[10.1038/s41467-022-34893-3](https://doi.org/10.1038/s41467-022-34893-3)
20. Otto H, Lamparter T, Borucki B, Hughes J, Heyn MP. Dimerization and inter-chromophore distance of Cph1 phytochrome from *Synechocystis*, as monitored by fluorescence homo and hetero energy transfer. *Biochemistry.* 2003;42(19):5885-5895.
21. Schenk A, Ivanchenko S, Röcker C, Wiedenmann J, Nienhaus GU. Photodynamics of red fluorescent proteins studied by fluorescence correlation spectroscopy. *Biophys J.* 2004;86(1):384-394.
22. Scheerer P, Michael N, Park JH, et al. Crystallization and preliminary X-ray crystallographic analysis of the N-terminal photosensory module of phytochrome Agp1, a biliverdin-binding photoreceptor from *Agrobacterium tumefaciens*. *J Struct Biol.* 2006;153(1):97-102.
23. McDonagh AF. Bile Pigments: Bilatrienes and 5,15-Biladienes. In: Dolphin D, ed. *The Porphyrins*. Academic Press; 1979:293-491.
24. Kapusta P, Erdmann R, Ortmann U, Wahl M. Time-resolved fluorescence anisotropy measurements made simple. *J Fluoresc.* 2003;13(2):179-183.
25. Lamparter T, Carrascal M, Michael N, Martinez E, Rottwinkel G, Abian J. The biliverdin chromophore binds covalently to a conserved cysteine residue in the N-terminus of *Agrobacterium* phytochrome Agp1. *Biochemistry.* 2004;43(12):3659-3669.
26. Lakowicz JR, ed. *Principles of Fluorescence Spectroscopy*. 2nd ed. Springer; 1999.
27. Schroder GF, Alexiev U, Grubmüller H. Simulation of fluorescence anisotropy experiments: probing protein dynamics. *Biophys J.* 2005;89(6):3757-3770.

How to cite this article: Elkurdi A, Guigas G, Hourani-Alsharafat L, et al. Time-resolved fluorescence anisotropy with Atto 488-labeled phytochrome Agp1 from *Agrobacterium fabrum*. *Photochem Photobiol.* 2023;00:1-12. doi:[10.1111/php.13851](https://doi.org/10.1111/php.13851)